Journal of the Air & Waste Management Association

ISSN: 1096-2247 (Print) 2162-2906 (Online) Journal homepage: http://www.tandfonline.com/loi/uawm20

Modeling and Direct Sensitivity Analysis of Biogenic Emissions Impacts on Regional Ozone Formation in the Mexico-U.S. Border Area

Alberto Mendoza-Dominguez , James G. Wilkinson , Yueh-Jiun Yang & Armistead G. Russell

To cite this article: Alberto Mendoza-Dominguez , James G. Wilkinson , Yueh-Jiun Yang & Armistead G. Russell (2000) Modeling and Direct Sensitivity Analysis of Biogenic Emissions Impacts on Regional Ozone Formation in the Mexico-U.S. Border Area, Journal of the Air & Waste Management Association, 50:1, 21-31, DOI: 10.1080/10473289.2000.10463987

To link to this article: http://dx.doi.org/10.1080/10473289.2000.10463987

Published online: 27 Dec 2011.

Submit your article to this journal

Article views: 106

View related articles

Citing articles: 6 View citing articles

Full Terms & Conditions of access and use can be found at
http://www.tandfonline.com/action/journalInformation?journalCode=uawm20

Download by: [University of North Texas] **Date:** 27 January 2017, At: 12:26

ISSN 1047-3289 *J. Air & Waste Manage. Assoc.* **50**:21-31

Copyright 2000 Air & Waste Management Association

Modeling and Direct Sensitivity Analysis of Biogenic Emissions Impacts on Regional Ozone Formation in the Mexico–U.S. Border Area

Alberto Mendoza-Dominguez, James G. Wilkinson, Yueh-Jiun Yang, and Armistead G. Russell
School of Civil and Environmental Engineering, Georgia Institute of Technology, Atlanta, Georgia

ABSTRACT

A spatially and temporally resolved biogenic hydrocarbon and nitrogen oxides (NO_x) emissions inventory has been developed for a region along the Mexico–U.S. border area. Average daily biogenic non-methane organic gases (NMOG) emissions for the 1700×1000 km^2 domain were estimated at 23,800 metric tons/day (62% from Mexico and 38% from the United States), and biogenic NO_x was estimated at 1230 metric tons/day (54% from Mexico and 46% from the United States) for the July 18–20, 1993, ozone episode. The biogenic NMOG represented 74% of the total NMOG emissions, and biogenic NO_x was 14% of the total NO_x. The CIT photochemical airshed model was used to assess how biogenic emissions impact air quality. Predicted ground-level ozone increased by 5–10 ppb in most rural areas, 10–20 ppb near urban centers, and 20–30 ppb immediately downwind of the urban centers compared to simulations in which only anthropogenic emissions were used. A sensitivity analysis of predicted ozone concentration to emissions was performed using the decoupled direct method for three dimensional air quality models (DDM-3D). The highest positive sensitivity of ground-level ozone concentration to biogenic volatile organic compound (VOC) emissions (i.e., increasing biogenic VOC emissions results in increasing ozone concentrations) was predicted to be in locations with high NO_x levels, (i.e., the urban areas). One urban center—Houston—was predicted to have a slight negative sensitivity to biogenic NO emissions (i.e., increasing biogenic NO emissions results in decreasing local ozone concentrations). The highest sensitivities of ozone concentrations to on-road mobile source VOC emissions, all positive, were mainly in the urban areas. The highest sensitivities of ozone concentrations to on-road mobile source NO_x emissions were predicted in both urban (either positive or negative sensitivities) and rural (positive sensitivities) locations.

IMPLICATIONS

This study describes an initial application of DDM-3D, a state-of-the-science sensitivity technique for three-dimensional air quality models, to the Mexico–U.S. border area to assess impacts of both biogenic and anthropogenic emissions on the air quality of the region. DDM-3D allows a much faster and more precise way of characterizing the impacts of different sources (biogenic and anthropogenic) throughout a domain. The application of DDM-3D provides information that can be used in source apportionment and control strategy development. This study also provides the first regional biogenic emissions inventory for northern Mexico.

INTRODUCTION

Transboundary air pollution between the United States and Mexico has received increasing attention from both countries since the late 1970s, leading to a number of cooperative programs to study this problem.[1-3] Further, with the passage of the North American Free Trade Agreement (NAFTA), interest has increased among various institutions in Mexico and the U.S. in developing an understanding of air pollution dynamics to evaluate the environmental impacts of NAFTA across the Mexico–U.S. border and in urban centers located near the border. Not only are such studies valuable for evaluating the impact of inter- and intra-country vehicular traffic and commercial and industrial activities on regional air quality, but they are also valuable for locating and quantifying sources of primary and secondary air pollutants. Ozone pollution, in particular, has proven to be difficult to abate in U.S.[4,5] and Mexican cities.[6] As shown in Figure 1, the metropolitan areas of Houston-Galveston-Brazoria, El Paso, and Dallas-Fort Worth in Texas and the region of Sunland Park in New Mexico, which is downwind of El Paso, are in nonattainment of the current 1-hr U.S. National Ambient Air Quality Standard (NAAQS) for ozone.[5] For cities in the border strip (Figure 1) besides El Paso, air quality information is scarce and is mainly reported for the Lower Rio Grande Valley. On the Mexican side of the domain, only Monterrey and Ciudad Juarez have routine air

quality monitoring networks. Monterrey and Ciudad Juarez have violated the Mexican ozone 1-hr standard of 110 ppb on average 22 and 15 days per year since 1993, respectively.[6] A proper characterization of anthropogenic and biogenic emissions is necessary to further understand the transport of pollutants across the border.

Ozone is formed in the troposphere by the reaction of nitrogen oxides (NO_x) with volatile organic compounds (VOCs) in the presence of sunlight.[7] The importance of biogenic VOC emissions on urban ozone formation was neglected in early photochemical air pollution studies based on (1) the assumption that biogenic emissions were small compared to anthropogenic emissions, and (2) the fact that, typically, biogenic VOC concentrations in an urban setting are much smaller than anthropogenic VOC.[8] Today, it is recognized that biogenic hydrocarbons can account for a large fraction of the total VOCs emitted in an airshed and that even in low concentrations, their high reactivity (or ozone formation potential) may have significant effects on ozone production.[9] For example, it has been reported that isoprene, α-pinene, and β-pinene, key emitted biogenic species, are more reactive than a weighted average of hydrocarbons emitted from anthropogenic sources.[10] Given that biogenic VOCs have a high reactivity compared to anthropogenic VOCs, in areas with high anthropogenic NO_x emissions, biogenic VOC emissions can help foster episodes of high ozone concentration.[4] On the other hand, biogenic nitric oxide (NO) emissions that result from soil microbial processes during the nitrification/denitrification cycle are exacerbated by soil fertilization activities[4] and can approach the anthropogenic NO flux of urban areas.[11,12]

Given the importance of biogenic emissions on ozone formation, it is prudent to develop reliable biogenic emissions inventories to follow regional ozone production. Biogenic emissions inventories for Mexico have been developed mainly for the metropolitan area of Mexico City.[13-15] There is, however, a great need to develop inventories for other regions of the country with air pollution problems. The objectives of this study are as follows: first, to develop a biogenic hydrocarbon and NO emissions inventory for the Mexico–U.S. border area; second, to integrate the biogenic inventory into a photochemical airshed model simulation to characterize the air pollution dynamics in the region; and third, to apply direct sensitivity analysis to assess the impacts of emissions on urban and rural ozone formation.

METHODS

This study focuses on the development of an episodic biogenic emissions inventory for the Mexico–U.S. border and

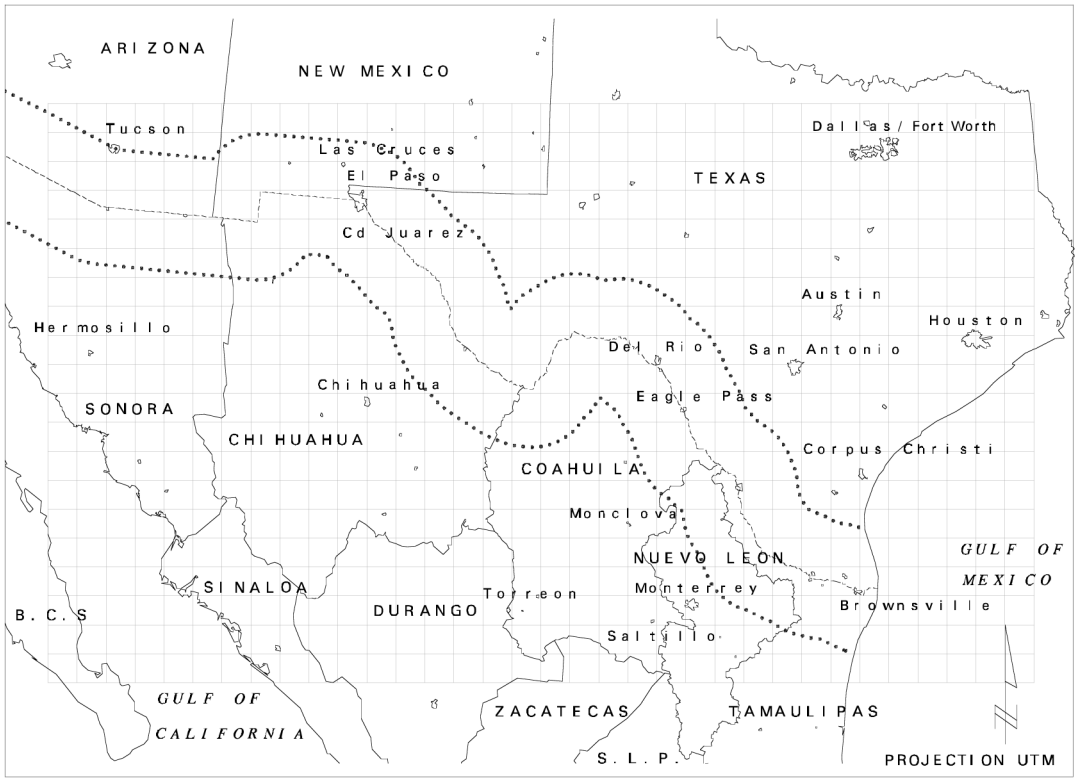

Figure 1. Map of the Mexico–U.S. border area, the location of major urban centers, and the extent of the modeling domain (for clarity of presentation, the size of the grid cells depicted are 50 × 50 km^2). The dashed solid line represents the international limit and the solid dotted line the extent of the border strip (100 km from each side of the international limit). State names are in upper case and city names in upper-lower case.

on the impacts of biogenic and anthropogenic emissions on urban and rural ozone production. A description of the main physiographical characteristics of the modeling domain is given in this section, followed by descriptions of the biogenic emissions modeling and the photochemical modeling frameworks.

The Mexico–U.S. Border Area

The Mexico–U.S. border is approximately 3200 km in length, extending from the Pacific Ocean to the Gulf of Mexico (Figure 1). Of note, the border area between Baja California (Mexico) and California (United States) is not included in this study. Approximately half of the border area, extending from the Ciudad Juarez–El Paso metropolitan area to the Gulf of Mexico, is delimited naturally by the Rio Grande, which is known as the Rio Bravo in Mexico.

The western boundary of the modeling domain is defined by the Sierra Madre Occidental and the Gulf of California, and the eastern boundary is defined by the Gulf of Mexico and the eastern plains of Texas. Two mountain chains divide the region: the Sierra Madre Occidental, which runs along the western coast of the Mexican mainland (with the Gulf of California) to southern Arizona; and the Sierra Madre Oriental, which runs from the vicinity of the city of Monterrey south along the border of the States of Nuevo Leon and Tamaulipas. Between the Sierras, the northern Mexican plateau (about 1300 m above sea level) extends north, becoming part of the great plains of North America. To the east of the Sierra Madre Oriental, the Gulf of Mexico plains also extend north.[16] Climates in the region are predominantly dry. The Sierras and the Gulf of Mexico plains have a temperate subhumid climate, with average temperature from 10 to 18 °C and annual rainfall from 600 to 1000 mm. The central plains are typically dry, with annual rainfall between 300 and 600 mm and average temperatures ranging between 18 to 22 °C. The eastern region of the state of Chihuahua, western Texas, and southeastern New Mexico are arid, with average annual rainfall less than 300 mm and mean temperatures between 18 and 26 °C.[16]

Coniferous oak forests dominate the Sierras of the west and east as well as the forests of eastern Texas. Between the Sierras and their respective coasts, dry tropical forests are predominant (i.e., tropical deciduous low forest and tropical thorn low forest). The central plateau is predominantly covered by arid and semiarid shrublands. Between the shrublands and the Sierra of the west there exists a transitional zone covered mainly by grasslands. Important agglomerations of halophilous vegetation, scrubland, and scrub woodland can be found in places over the central plateau.[16]

Biogenic Model

The U.S. Environmental Protection Agency's (EPA) second version of the Biogenic Emissions Inventory System (BEIS2) was used to estimate biogenic VOC emissions. The environmental algorithm used by BEIS2 was developed by Guenther et al.[17] This algorithm corrects the effects of temperature and solar radiation on biogenic VOC emissions. A complete description of the algorithm used by BEIS2 can be found elsewhere.[18] For biogenic NO, the model developed by Williams et al.[19] was used.

The general approach to estimating biogenic VOC emissions rates is to combine emissions factors, which are a function of temperature and photosynthetically active radiation (PAR), with a database containing the amount of earth's surface covered by the biomes of the region of interest.[4] Biogenic emissions are estimated via eq 1.[20]

$$E = E_S \cdot C_f \cdot A \tag{1}$$

where E is the meteorological-specific emission rate (µg hr^{-1} ha^{-1}), E_S is the species-specific emission flux at 30 °C and 1000 µmole m^{-2} sec^{-1}, C_f is the hourly species-specific environmental correction factor, and A is the area of species coverage. For isoprene emissions, C_f is calculated as

$$C_f = C_L \cdot C_T \tag{2}$$

$$C_L = \frac{\alpha \cdot c_{L1} \cdot L}{\sqrt{1+\alpha^2 \cdot L^2}} \tag{3}$$

$$C_T = \frac{\exp\left(\dfrac{c_{T1}(T-T_s)}{R \cdot T_s \cdot T}\right)}{1+\exp\left(\dfrac{c_{T2}(T-T_s)}{R \cdot T_s \cdot T_M}\right)} \tag{4}$$

where C_L is the light intensity correction factor, C_T is the temperature correction factor, L is the PAR flux (µmole m^{-2} sec^{-1}), c_{L1} and α are empirical coefficients derived from emission rate measurements,[17] T is the leaf temperature (taken to be ambient temperature, K), R is the ideal gas constant, T_s is the normalizing temperature (303 K), and T_M, c_{T1}, and c_{T2} are empirical coefficients derived by fit to species of several genera.[17]

In the case of monoterpenes and other VOCs (OVOC), the environmental correction factor, C_f, is given as

$$C_f = \exp\left(\beta \cdot (T - T_s)\right) \tag{5}$$

where β is an empirical coefficient derived by fit to species of several genera.[17] Finally, for the case of NO emissions, C_f is estimated by

$$C_f = \exp(T_3 \cdot T_{soil}) \quad (6)$$

where T_3 is an empirical parameter derived from emissions rate measurements (°C^{-1}) and T_{soil} is the soil temperature which is dependent on land use (°C). T_{soil} is computed as

$$T_{soil} = T_1 \cdot T + T_2 \quad (7)$$

where T_1 is an empirical parameter derived from emissions rate measurements and T_2 is a land use-specific soil temperature adjustment factor (°C). This formulation basically requires three set of inputs: the area of species coverage (A), and temporally and spatially resolved temperature and PAR fields.

Inputs to the Biogenic Model

The species coverage (A) for the United States was derived from the Biogenic Emissions Landcover Database (BELD) and the Land Cover Characteristics (LCC25) coverage.[21] The BELD is a table containing coverage estimates of 127 plant communities and species resolved to the county level for the United States. The BELD divides the county data into four main categories: rural forest cover, agricultural cover, urban forest cover, and other land covers. The LCC25 digital coverage contains 27 classes of species coverage for the United States and is used as a surrogate to allocate spatially data from the BELD.

Two data sets were created, similar to the BELD and LCC25, to represent Mexican vegetation. This was done to use the same software and for consistency with the U.S. data. Maps (scale 1:1,000,000) from the National Institute of Statistics, Geography, and Informatics (INEGI) were used to develop vectorized digital land use/land cover data for Mexico. Since INEGI's classification differs from the one used by the BELD and LCC25, the Mexican data set was preprocessed before being integrated to the final database. The Mexican BELD was constructed by assigning plant communities in the INEGI data to those that exist in the U.S. BELD data set. Further, the Mexican BELD was resolved to the municipality level, which is similar to a U.S. county. The guidelines for the integration were taken from Rzedowski's description of the Mexican vegetation types.[22] Agricultural coverage data at the municipality level for Mexico were obtained from the Sistema Nacional de Información Agropecuaria released by the Centro de Estadística Agropecuaria (CEA) of the Department of Agriculture, Livestock, and Rural Development (SAGAR)[23] and from the Sistema Municipal de Base de Datos (SIMBAD)[24] operated by INEGI. Species-specific crop areas for the spring-summer cycle of 1993 were used. Agricultural species that were allocated for each municipality were cotton, rice, oat, barley, corn, sorghum, soybean, wheat, alfalfa, orange (citric), and hay. The remaining agricultural species were assigned to the "miscellaneous crops" category because no similar species are available in the U.S. BELD. Vegetation for Mexican urban areas was not available, and it was assumed that the areas were composed of 20% mixed urban forest and 20% grasslands. The Mexican LCC25 digital map was created using an existing cross-reference table between the United States Geological Survey (USGS) and INEGI's land use classifications.[25] Note that no specific emission factors for Mexican vegetative species were included because little research has been undertaken to describe the emissions characteristics of plant species specific to Mexico.

Input data for the biogenic model was completed with the specification of the meteorological variables. The PAR field was computed in two steps. First, clear sky total radiation values were computed based on the work of Iqbal.[26] PAR that falls in the visible spectrum of 400–700 *n*m was taken as half of the total radiation.[20] Second, the PAR field was scaled using a cloud cover field. The temporally and spatially resolved cloud cover and temperature fields were generated using an objective analysis technique[27] with data from 95 monitoring stations.[25]

Photochemical Air Quality Modeling and Sensitivity Analysis

The air quality model used in this study to predict ozone formation is the California/Carnegie Institute of Technology (CIT) model. This Eulerian model has been used previously to address photochemical air pollution issues in different urban[13, 28-30] and regional (i.e., the Mexico–U.S. border[25] and the Swiss Plateau[31]) areas. The CIT photochemical airshed model simulates the formation and transport of photochemical air pollution by solving the atmospheric diffusion equation[32]

$$\frac{\partial c_i}{\partial t} = -\nabla \cdot (\mathbf{u} c_i) + \nabla \cdot (\mathbf{K} \nabla c_i) + R_i(c_1, c_2, ..., c_n; T, t) + S_i \qquad i = 1, ..., I \quad (8)$$

where $c_i(x,t)$ represents the ensemble average concentration of species i, K is the turbulent diffusion tensor, $u(x,t)$ is the advective field, R_i is the gas phase reaction rate of species i, and S_i is the elevated point-source rate of emissions of species i, $T(x,t)$ is the temperature, t is the time vector, and x is the position vector. The formulation is subject to boundary and initial conditions (not shown here) to solve the equation. Details of the model formulation are described elsewhere.[28, 33-34] Finally, in this study, the VOC-NO_x chemistry is treated via the SAPRC90 chemical mechanism.[35]

A unique feature of the CIT model is its ability to calculate sensitivity coefficients of model outputs to model parameters and inputs through the use of the decoupled

direct method for three dimensional models (DDM-3D).[36] DDM-3D allows calculation of sensitivity coefficients in a computationally efficient fashion. The sensitivity coefficients are computed through the derivative of the model output (i.e., species concentration, c_i) with respect to a semi-normalized model input or parameter (i.e., $\varepsilon_j = p_j/p_j^o$, where ε_j is a scaling variable with a nominal value of 1; p_j is the scaled model parameter [e.g., rate constant] or model input [e.g., area source emissions]; and p_j^o is the nominal value of the model parameter or model input). This results in an auxiliary equation, which is very similar to the atmospheric diffusion equation

$$\frac{\partial s_{ij}^*}{\partial t} = -\nabla\cdot\left(\mathbf{u}s_{ij}^*\right) + \nabla\cdot\left(\mathbf{K}\nabla s_{ij}^*\right) + J_{ik}s_{kj}^* + \frac{\partial R_i}{\partial \varepsilon_j} + \frac{\partial S_i}{\partial \varepsilon_j} - \nabla\cdot\left(\mathbf{u}c_i\right)\delta_{ij} + \nabla\cdot\left(\mathbf{K}\nabla c_i\right)\delta_{ij} \tag{9}$$

where J is the Jacobian matrix defined as $J_{ik} = \partial R_i/\partial c_k$. The last two terms are production due to wind speed (u) and diffusivity (K), and they exist only if sensitivity to wind speed and diffusivity are applied. Similar equations can be developed for boundary and initial conditions, although details of this derivation are found elsewhere.[36] With this approach, the model can be applied once, and the sensitivity fields of all the pollutants to different emission sources can be calculated simultaneously. The method has been previously used in two urban domains: Los Angeles[36] and Atlanta.[29] Further, DDM-3D not only provides temporally and spatially resolved sensitivity fields, but it can also be used in source attribution analyses and to develop emissions control strategies.[29,37]

DDM-3D has two main advantages over applying a brute-force approach (i.e., where a base simulation is run along with a second simulation where the input or model parameter has been perturbed, and the sensitivity is found by computing the difference between the two). First, it is much faster. Yang et al.[36] found that for an application to the South Coast Air Basin of California one could solve for the sensitivity of all pollutant concentrations to 20 inputs with a very modest (80%) increase in computational time over a base simulation. In this study, it was found that a single parameter sensitivity analysis required two times the execution time relative to concentration calculations alone; a five-parameter sensitivity analysis required roughly three times the execution time. In the last case, the brute-force approach would have required six times the execution time. As noted here and in the Los Angeles study,[36] the increment in execution time from one run to another is lower as more parameters are added. The second advantage of DDM-3D is that the sensitivity field computed is numerically more stable than the brute-force approach.[36]

The modeling domain is $1000 * 1700$ km^2 in the horizontal (Figure 1) with a grid cell size of 12.5×12.5 km^2. There are six vertical layers: 0–30, 30–100, 100–300, 300–700, 700–1500, and 1500–3100 m above ground level. The model was applied to a summer episode, July 18–20, 1993, which had peak observed ozone levels of 102 ppb in the Monterrey metropolitan area. The CIT model performance evaluation for ozone was conducted following EPA procedures, and it was complemented by guidelines suggested by Tesche et al.[38] The model inputs are described thoroughly by Mendoza et al.[25] Anthropogenic emissions are described by Mejia et al.[39] The emission inventory was complemented with the biogenic emissions calculated in this study. In addition to the work described here, sensitivity tests were also conducted to assess the impact of model resolution using grid cells ranging from 6.25×6.25 km^2 to 50×50 km^2. Similar results were found for simulations conducted using 6.25×6.25 km^2 to 25×25 km^2 cells.[25] More significant differences were encountered when using 50×50 km^2 cells.[25]

RESULTS AND DISCUSSION

Biogenic Emission Inventory

Eighty percent of the domain, 170 x 10^6 ha, is covered by land. Of this area, 57% is Mexican territory and 43% is U.S. territory. Table 1 summarizes the areal extent of the six main land use categories. The predominant vegetation classes are the desert brushlands and grasslands, with Mexico covered by a fair amount of barren land. Figures 2a and 2b depict the spatial distribution of two land use classes presented in Table 1: rural forest and agricultural areas. As shown in Figure 2a and discussed earlier, the forests are located along the western coast of Mexico parallel to the Gulf of California (the Sierra Madre Occidental), in northeastern Mexico where the northernmost part of the Sierra Madre Oriental exists, and in eastern Texas. The primary agricultural areas (Figure 2b) are located near the heavily urbanized areas. Note that the central plateau lacks forest and agricultural that are covered mainly by desert brush.

The spatial distribution of the biogenic emission estimates for the third day of the episode are presented in

Table 1. Areal extent (hectares) of different land use classes within the modeling domain.

Land Use	Mexico	United States
Agricultural area	4,915,740	12,151,040
Barren land	6,073,050	2,754,630
Forest land	18,449,160	8,456,250
Urban forest land	447,020	319,040
Other[a] vegetation types	47,471,900	34,060,580
Water[b]	356,120	809,350

[a]Includes mainly grassland and desert shrubland. [b]Includes only inland water bodies.

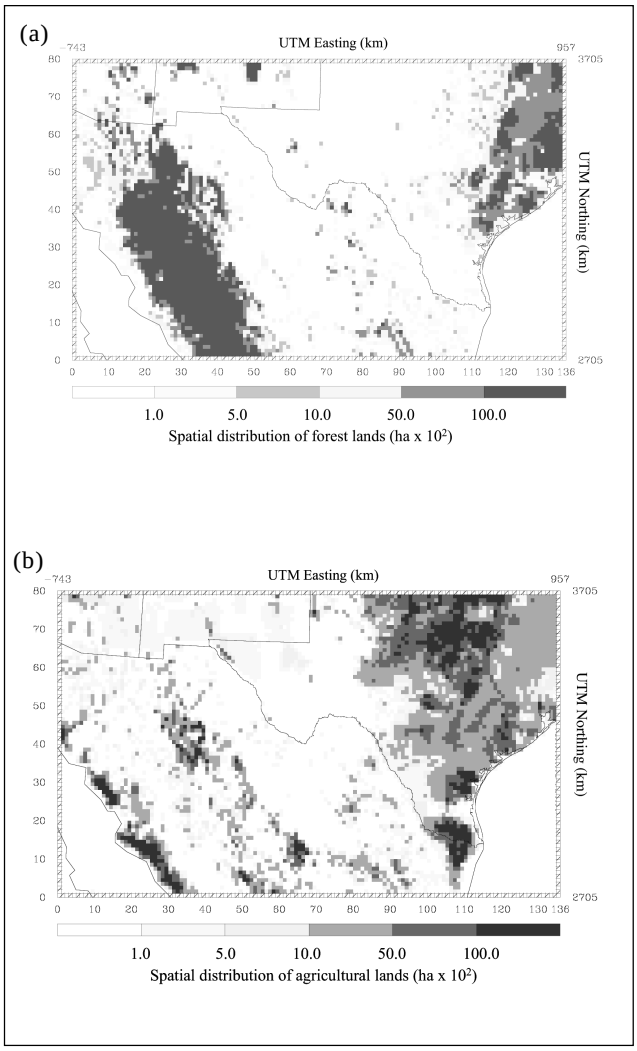

Figure 2. Spatial distribution of (a) forest and (b) agricultural lands in the modeling domain. Values represent surface covered (in ha $\times$ 10^2) by the corresponding land use class in each cell. Each grid cell is 12.5 $\times$ 12.5 km^2 for a total area of 15,625 ha.

Figure 3. Figures 3a, 3b, and 3c depict the emissions for the VOC species (isoprene, monoterpenes, and OVOC), while Figure 3d depicts the NO emissions. The areas of major hydrocarbon emissions closely follow the forest locations shown in Figure 2a. Differences in the magnitude of emissions correspond to the local mix of tree species. Monoterpenes and OVOC are also emitted in fair amounts in non-forested areas (e.g., south-central Texas, northeast Mexico, South Arizona, and northern Sonora), where the vegetation is mainly composed of shrub, scrub, and agricultural species. Biogenic hydrocarbon emissions are negligible in the desert. Biogenic NO is heavily emitted in agricultural areas, although there are exceptions, most notably in eastern Texas. Biogenic NO emissions are considerably lower in heavily forested, urbanized, and desert areas.

Table 2 summarizes the domain-wide biogenic emissions for the three-day episode. Of the total biogenic

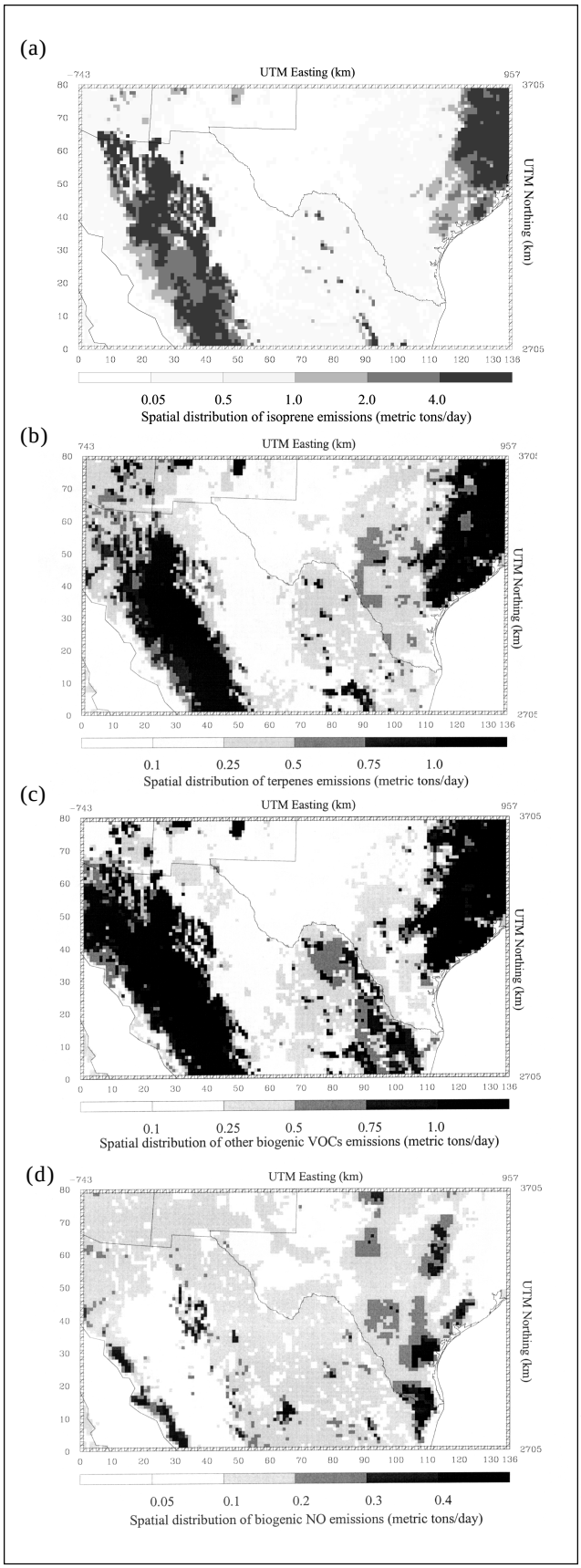

Figure 3. Gridded biogenic emissions, in metric tons per day, using 12.5 $\times$ 12.5 km^2 grid cells, for the third day of simulation (July 20, 1993): (a) isoprene, (b) terpenes, (c) other biogenic VOCs, and (d) biogenic NO.

non-methane organic gases (NMOGs) emitted in the domain, 62% is released from Mexico and 38% from the U.S. In the case of biogenic NO, 54% is from Mexico and 46% from the U.S. Table 3 compares the biogenic emissions computed in this study with the anthropogenic emissions calculated by Mendoza et al.[25] for the same domain. The biogenic NMOG represent roughly 74% of the total NMOG emissions, while biogenic NO_x is 14% of the total NO_x.

Photochemical Modeling Results

The biogenic emission estimates from this study were added to an existing anthropogenic emissions inventory for the same modeling domain, and the CIT model was used to predict ozone concentrations. The observed peak ozone concentrations did not exceed 120 ppb in the United States and did not exceeded 110 ppb in Mexico. In light of the 8-hr standard for ozone being proposed by EPA, 8-hr running averages of ozone concentration were calculated. No station exceeded 80 ppb as an 8-hr average. Monterrey, Dallas-Fort Worth, Ciudad Juarez-El Paso, and Houston each had several episodes where the 8-hr ozone average was in the range of 71–75 ppb. Nevertheless, the results are important in the context of analyzing the dynamics of pollutants in this regional domain during non-extreme conditions. This is important in regard to ozone exposure and to the impact of NO_x and VOC emissions on that endpoint. Figure 4 depicts the daily predicted maximum ozone concentration for the third day of the episode (July 20, 1993). The third day was selected in order to minimize the influence of the initial conditions on the analysis. As shown in Figure 4, the ozone plumes from the major urban areas—Houston, Dallas-Fort Worth, San Antonio, and Austin in the United States, and Monterrey, Torreon, and Chihuahua in Mexico—can be identified. Within the border strip, ozone levels build up in the Matamoros/Brownsville-Reynosa/McAllen industrial corridor (in the southernmost tip of Texas) and especially in the Ciudad Juarez-El Paso area, where the plume is transported to the north across the border. Also, within the border strip, ozone levels build up near the Ciudad Acuña/Del Rio–Piedras Negras/Eagle Pass corridor. Note that the Carbon I and Carbon II electrical generating units are located about 30 km south of Piedras Negras. Carbon I has four coal-fired units that generate 300 MW each; Carbon II has two coal-fired units that produce 350 MW each.

Several statistics that compare the predicted ozone concentrations to the observations were calculated to assess the performance of the model. By EPA guidelines, the model should predict the observed peak ozone (unpaired in time and space) within ±15–20%, have an overall bias of ±5–15%, and have a gross error of 30–35%.[38] The normalized mean square error (NMSE), another statistic that has relevance in model performance evaluation but is seldom examined in air quality modeling studies, is a robust measure of overall model performance where values less than 0.4 indicate good model performance.[20] The systematic/unsystematic occurrence of the errors can be analyzed through the root mean square error (RMSE). The RMSE can be divided into two components, a systematic RMSE ($RMSE_S$) and an unsystematic RMSE ($RMSE_U$), as follows:

$$RMSE^2 = RMSE_S^2 + RMSE_U^2 \qquad (10)$$

The $RMSE_S$ is a measure of a model's linear (or systematic) bias, and the $RMSE_U$ is a measures of the discrepancy between observations and predictions due to random processes outside the legitimate range of the model.[40,41] Table 4 presents statistics calculated for the last day of the episode. The bias indicates a tendency of the model to overpredict ozone concentrations. The peak accuracy

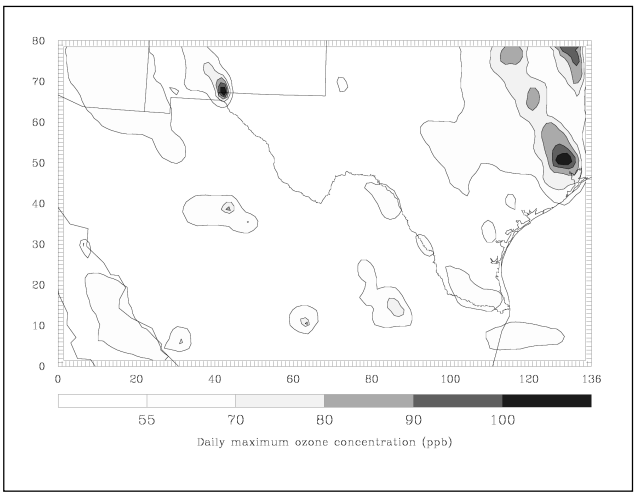

Figure 4. Maximum ground-level ozone concentration (ppb) for the third day of simulation (July 20, 1993).

Table 2. Biogenic NO and hydrocarbon emissions (metric tons/day) in the modeling domain contributed by each country during each day of the episode.

Emitted	1st Day		2nd Day		3rd Day	
Class	Mexico	U.S.	Mexico	U.S.	Mexico	U.S.
Nitric oxide	679	561	678	558	662	569
Isoprene	8,506	3,565	8,171	3,615	6,945	3,745
Monoterpenes	3,157	2,517	3,170	2,512	2,982	2,605
OVOC	3,751	2,874	3,766	2,866	3,548	2,973

Table 3. Emission totals (metric tons/day) by source in the modeling domain for July 20, 1993.

Source	NO_x	NMOG	CO	SO_x
Area sources	1,623	1,901	5,109	445
Biogenic sources	1,231	22,798	-	-
Mobile sources	2,464	5,101	16,718	147
Point sources	3,215	1,015	2,099	5,137
Total	8,533	30,815	23,926	5,729

(unpaired) and the gross error fall in the range of EPA guidelines, and the NMSE indicates that the model performs well across the range of observed ozone. Of the peak accuracy estimates, the unpaired peak accuracy (AU) produces the best result, although it is the least stringent of the model performance tests and is most questionable as to being a good measure of model performance. Though values for the peak estimation accuracy paired in time and space (ATS) and peak estimation accuracy paired in space (AS) were poor, peak estimation paired in time (AT) performed well. Figure 5 presents a time series plot of the RMSE, with its systematic and unsystematic components. The systematic RMSE dominates the total RMSE during the day, precisely when photochemistry drives the atmospheric reactions. This suggests that a refinement of the inputs to the model is warranted and should be sought for future applications. Note that the daytime RMSE is at its lowest during the third day.

Mendoza et al.[25] conducted a simulation of the same episode employing only anthropogenic emissions. In order to compare the runs, the maximum difference in ozone concentration at each grid cell between the run with biogenics and the one without biogenics was computed and plotted (Figure 6). In general, ozone increased 20–30 ppb in most of the major urban centers, 10–20 ppb in some urban and most suburban areas, and less than 10 ppb in rural areas. The maximum increase, approximately 40 ppb, was predicted in Ciudad Juarez–El Paso and eastern Texas. Table 4 also presents the performance statistics obtained from the run without the biogenic emissions. From a model performance perspective, the model run with biogenic

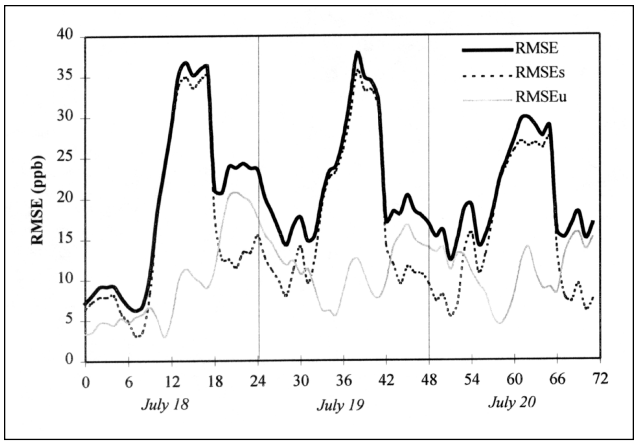

Figure 5. Time series plot of the root mean square error (RMSE) statistic for ozone, including its systematic and unsystematic components.

emissions gave better results for the ATS, AS, and AT statistics, and NMSE values remained comparable (0.10 with biogenics versus 0.09 without), although the run with biogenics had a greater tendency to overpredict ozone as noted by a higher, positive bias. It should be noted that the anthropogenic emissions inventory was estimated based on emissions from a typical summer day rather than from day-specific data. Corrections due to ambient conditions for this non-extreme episode may have been inaccurate, leading to overestimation of some anthropogenic VOC classes (e.g., evaporative mobile emissions).

Sensitivity Analysis

The sensitivity of ozone concentration to anthropogenic area source emissions and biogenic emissions was performed using DDM-3D.[29,36] Sensitivities to the following emissions classes were computed: biogenic isoprene, α-pinene, and NO, and anthropogenic on-road mobile source NO_x and VOC. It has to be noted that DDM-3D computes linear (first order) sensitivity coefficients that are valid over a range of approximately 30% of changes in the base case emissions. Further, the reported sensitivities are expressed as a percent increase in emissions, though the results are not constrained to increments in emissions and are valid also to analyze emission reductions. In other

Table 4. Model performance evaluation for the third day of simulation.[a]

Statistic Group	EPA Guideline	Statistical Measure	Biogenics Run	No Biogenics Run
Peak accuracy		Peak estimation accuracy paired in time and space (ATS)	-41.3%	-48.1%
		Peak estimation accuracy paired in space (AS)	-36.9%	-43.2%
		Peak estimation accuracy paired in time (AT)	-23.1%	-29.4%
	< + 15-20%	Peak estimation accuracy unpaired (AU)	19.6%	7.8%
Bias statistics	< + 5-15%	Normalized bias	27.1%	0.7%
		Mean bias	12.8 ppb	-1.49 ppb
Error statistics	< + 30-35%	Normalized error	32.7%	24.5%
		Normalized mean square error	0.10	0.09

[a]Cutoff = 40 ppb.

words, a positive sensitivity coefficient due to an increase in a source category can be also interpreted as a negative sensitivity due to a decrease in the same source category. This provides information to source attribution analyses.

Figures 7a, 7b, and 7c present the ozone sensitivity fields to emissions of biogenic isoprene, α-pinene, and NO, respectively, at 3:00 p.m. on July 20, 1993. The sensitivities shown in Figure 7 present the predicted change in ozone (ppb) per 1% domain-wide increase in the corresponding emissions. An increase in isoprene emissions tends to increase ozone levels in areas where the anthropogenic NO_x emissions are relatively higher (e.g., eastern Texas, Monterrey, and Tucson). In contrast, ozone has lower sensitivities to α-pinene emissions in urban and suburban areas because α-pinene is less reactive than isoprene. The sensitivity field in rural areas remains higher for α-pinene than for isoprene, however, due to a more extended emissions coverage for α-pinene. In general, the ozone sensitivity fields for α-pinene and isoprene are spatially similar, although a major difference is the negative ozone sensitivity along the western Mexican Sierras for α-pinene. Trainer et al.[42] reported that under conditions of low NO_x emissions, biogenic isoprene can lead to a slight reduction in ozone. To investigate the ozone negative sensitivity to α-pinene, kinetic rates for the two most important isoprene and α-pinene oxidation routes (reaction with ozone and the $HO^{\bullet}$ radical) were calculated in a typical cell (30, 40) located in the negative sensitivity band. The loss rates are computed as follows:

$$\frac{k_{isoprene-O_3}\left[O_3\right]}{k_{isoprene-HO^{\bullet}}\left[HO^{\bullet}\right]} \cong 0.16$$

$$\frac{k_{\alpha-pinene-O_3}\left[O_3\right]}{k_{\alpha-pinene-HO^{\bullet}}\left[HO^{\bullet}\right]} \cong 1.75$$

where $k_{X\text{-}Y}$ refers to the rate constant for the reaction of species X with species Y , and $[O_3]$ and $[HO^{\bullet}]$ are the concentrations of ozone and hydroxyl radical. One-hour average concentrations and temperature at 3:00 p.m. were adopted for the loss rate calculations. According to the loss rates, isoprene will react faster with $HO^{\bullet}$ radicals, leading to the creation of $RO_2^{\bullet}$ radicals, which convert NO to nitrogen dioxide (NO_2) without destroying an ozone molecule. On the other hand, α-pinene reacts faster with ozone than with hydroxyl radicals, producing peroxyacyl radicals[35] that act as sinks for odd nitrogen, effectively retarding the rate of ozone production.[43] The consumption of O_3 by α-pinene and the removal of odd

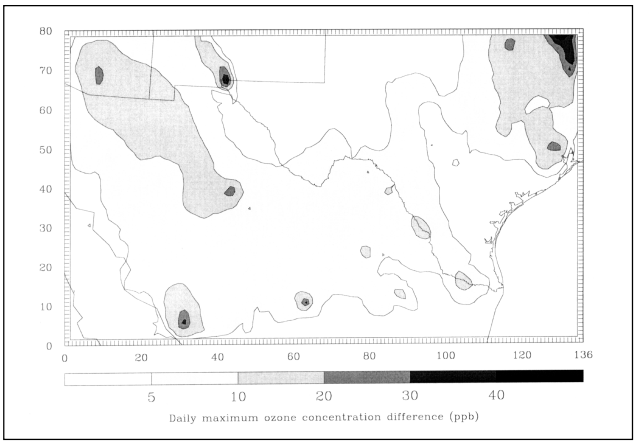

Figure 6. Maximum ground-level ozone concentration difference (ppb) between the simulation with biogenic emissions and the simulation without. Third day of simulation (July 20, 1993).

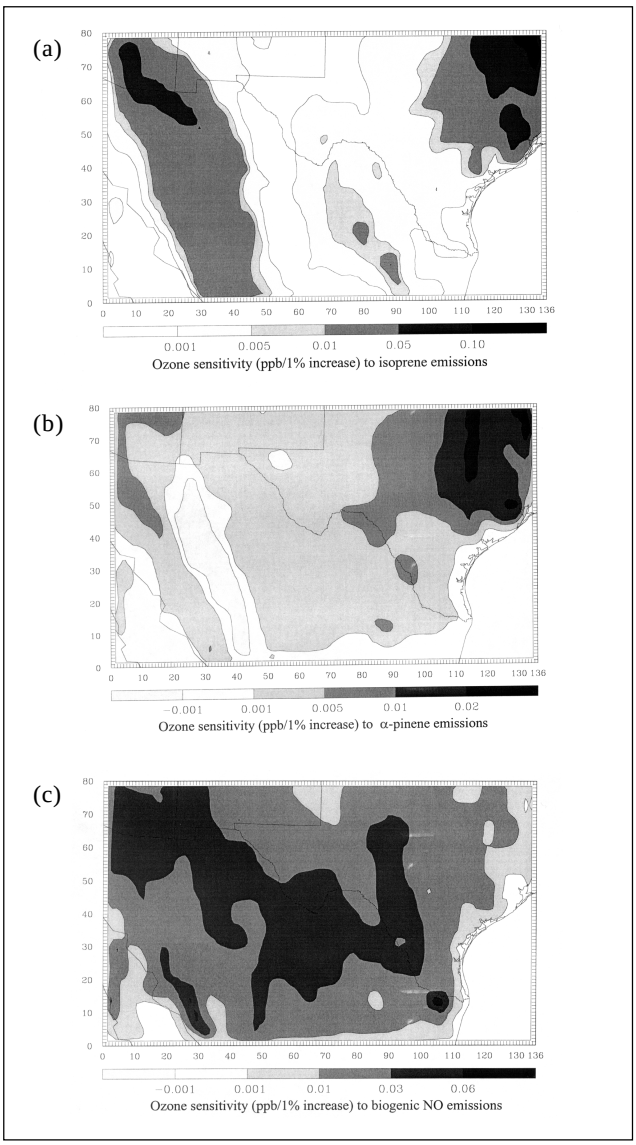

Figure 7. Sensitivity of ground-level ozone concentration to increases in biogenic emissions at 15:00 hr for the third day of simulation (July 20, 1993): (a) isoprene, (b) α-pinene, and (c) NO.

nitrogen contribute to the negative ozone sensitivity to α-pinene emissions.

The sensitivity of ozone to biogenic NO emissions is presented in Figure 7c. The results show that ozone is sensitive to increases of biogenic NO emissions in rural locations, and large sensitivities are found in some urban areas. Maximum sensitivities are located in two heavily agricultural areas: the Lower Rio Grande Valley and the coast of the State of Sinaloa, Mexico. A small portion of ozone sensitivity (not clearly appreciated in Figure 7c) was negative in the Houston metropolitan area because of strong NO_x inhibition. Figure 7 indicates that increasing biogenic NO emissions generally increases ozone levels in nonforested areas one order of magnitude (on a percent increase basis) more than the ozone increase due to biogenic VOC emissions.

Figures 8a and 8b illustrate the ozone sensitivities to mobile source VOC and NO_x emissions, respectively. Figure 8a indicates that ozone concentrations increase in urban centers and industrial corridors as mobile source VOC emissions increase. Remote rural locations have negligible ozone sensitivity to mobile source VOC emissions. Ozone sensitivity to mobile source NO_x emissions (Figure 8b) shows that the major urban cores (Ciudad Juarez-El Paso, Houston, Dallas-Fort Worth, San Antonio, Monterrey-Saltillo) present a NO_x-inhibiting atmosphere and that downwind areas of these urban cores present a NO_x-limited atmosphere. However, it has to be acknowledged that beyond a certain reduction in the NO_x emissions, the NO_x-inhibited areas will shift to NO_x-limited conditions. A comparison of ozone sensitivity to mobile source VOC and NO_x emissions indicates that increases in VOC emissions have a more noticeable impact on ozone levels in the immediate rural and suburban areas surrounding the urban cores than in the remote rural areas. In contrast, increases in mobile source NO_x emissions tend to have a higher impact in both urban and rural locations. Moreover, rural ozone sensitivity can differ by one order of magnitude depending on whether on-road mobile source NO_x or VOC increases. Results presented here are in agreement with findings of previous studies on the effect of biogenic emissions in rural ozone modeling.[44-46] Moreover, the results obtained here are important in that they can be used to analyze the impact of using NO_x control strategies against VOC control strategies. The inclusion of biogenic sources represents more realistically the VOC and NO_x loading that the different areas present. The absence of biogenic emissions will cloud any source impact analysis developed.

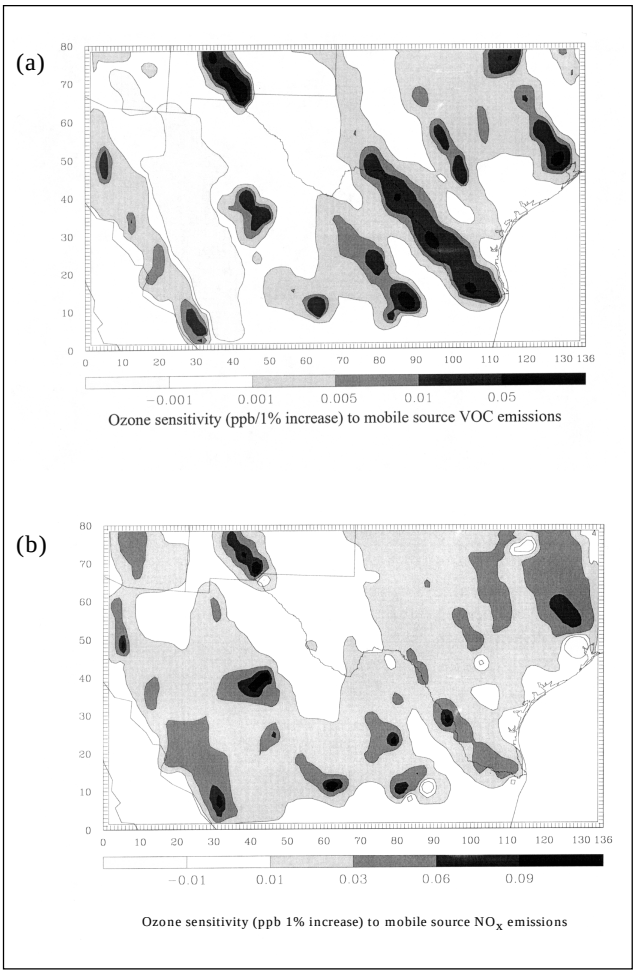

Figure 8. Sensitivity of ground-level ozone concentration to increases in anthropogenic emissions at 15:00 hr for the third day of simulation (July 20, 1993): (a) mobile VOC and (b) mobile NO_x.

CONCLUSIONS

An episodic biogenic emissions inventory was developed for a region along the Mexico–U.S. border using the BEIS2 and the model of Williams et al.[19] The biogenic emissions inventory was developed for the particular conditions of July 18–20, 1993. Biogenic NMOG and NO emissions in the domain are slightly higher in Mexico than in the United States. The new biogenic emissions inventory was integrated with an existing anthropogenic emissions inventory of the same domain to assess air quality better over the Mexico–U.S. border area using the CIT photochemical airshed model. The biogenic NMOG represents about 74% of the total NMOG emissions, and biogenic NO_x contributes about 14% of the total NO_x. The model performance evaluation for ozone shows that the model performs within acceptable limits using 12.5×12.5 km^2 grid cells, though in general the model tends to overpredict ozone. The predicted ground-level ozone levels increased compared to a previous study of the same domain, where anthropogenic emissions were used exclusively. The ozone increase ranges from 5–10 ppb in rural areas, 10–20 ppb near urban centers, and 20–30 ppb in most cities. A maximum ozone increase of 40 ppb was found in the Ciudad Juarez-El Paso metropolitan area and eastern Texas. Direct sensitivity analyses was then used to assess the

impact of emissions changes on ozone. The sensitivity of ground-level ozone concentration showed that changes in biogenic VOC emissions have the greatest impact on the ozone levels in the urban areas, whereas changes in mobile source VOC emissions have the greatest effect in rural locations immediately near urban areas. Changes in mobile source NO_x emissions impact both urban and rural areas.

ACKNOWLEDGMENTS

This study was supported by the National Science Foundation (Contract No. BES-9613729) and Georgia Power. Mendoza-Dominguez also acknowledges the *Consejo Nacional de Ciencia y Tecnología* (CONACYT) for partial support during his research stay at the Georgia Institute of Technology.

REFERENCES

1. *Convenio entre los Estados Unidos Mexicanos y los Estados Unidos de América sobre Cooperación para la Protección y Mejoramiento del Medio Ambiente en la Zona Fronteriza*; Secretaría de Desarrollo Urbano y Ecología, U.S. Environmental Protection Agency: La Paz, México, 1983.
2. *Plan Integral Ambiental Fronterizo: Primera Etapa 1992–1994*; Secretaría de Desarrollo Urbano y Ecología: México, 1992.
3. Tovar, D.; Gilbreath, J.: *Clean Energy along the Texas-Mexico Border: Building Consensus in Protecting Air Quality.* U.S.-Mexican Briefing Paper No. 1, U.S.-Mexican Policy Studies Program, LBJ School of Public Affairs, The University of Texas at Austin: Austin, TX, 1995.
4. National Research Council. *Rethinking the Ozone Problem in Urban and Regional Air Pollution*; National Academy Press: Washington, DC, 1991.
5. *National Air Quality and Emissions Trends Report*; EPA 454/R-97-013; U.S. Environmental Protection Agency: Research Triangle Park, NC, 1998.
6. Instituto Nacional de Ecología. *Primer Informe sobre la Calidad del Aire en Ciudades Mexicanas*; Dirección General de Gestión e Información Ambiental: México, 1997.
7. Seinfeld, J.H. *Science* **1989**, *243*, 745-752.
8. Chameides, W.L.; Lindsay, R.W.; Richardson, J.; Kiang, C.S. *Science* **1988**, *241*, 1473-1475.
9. Russell, A.; Milford, J.; Bergin, M.S.; McBride, S.; McNair, L.; Yang, Y.; Stockwell, W.R.; Croes, B. *Science* **1995**, *269*, 491-495.
10. Carter, W.P.L. *J. Air & Waste Manage. Assoc.* **1994**, *44*, 881-899.
11. Shepherd, M.F.; Barzetti, F.S.; Hastie, D.R. *Atmos. Environ.* **1991**, *25A*, 1961-1969.
12. Williams, E.J.; Parrish, D.D.; Buhr, M.P.; Fehsenfeld, F.C. *J. Geophys. Res.* **1988**, *93*, 9539-9546.
13. *Mexico City Air Quality Research Initiative—Modeling and Simulation*; Instituto Mexicano del Petroleo and Los Alamos National Laboratory: Mexico City, 1993; Vol. 3.
14. Cruz-Nunez, X.; Alegre-Gonzalez, M.V.; Castellanos-Fajardo, L.A. *The Emission Inventory: Programs & Progress*; Air & Waste Management Association: Pittsburgh, PA, 1995; pp 153-163.
15. Ruiz-Suarez, L.G.; Longoria, R.; Hernandez, F. In *Proceedings of the 1997 5th International Conference on Air Pollution*; Bologna, Italy, 1997; pp 923-933.
16. Instituto Nacional de Estadística Geografía e Informática. *Geographical Information of Mexico*; http://www.inegi.gob.mx/homeing/geografia/geograf.html (accessed 1998).
17. Guenther, A.; Zimmerman, P.R.; Harley, P.C.; Monson, R.K.; Fall, R. *J. Geophys. Res.* **1993**, *98*, 12609-12617.
18. Geron, C.T.; Guenther, A.B.; Pierce, T.E. *J. Geophys. Res.* **1994**, *99*, 12773-12791.
19. Williams, E.J.; Guenther, A.; Fehsenfeld, F.C. *J. Geophys. Res.* **1992**, *97*, 7511-7519.
20. Wilkinson, J.G. In *Proceedings of the NATO Advanced Research Workshop on Air Pollution in the Ural Mountains: Environmental, Health and Policy Aspects;* Magnitogorsk, Russia, 1997; pp 315-340.
21. Kinnee, E.; C.D. Geron, C.D.; Pierce, T.E. *Ecological Applications* **1997**, *7*, 46-58.
22. Rzedowski, J. *Vegetación en México*; Editorial Limusa: México, 1978.
23. Secretaría de Agricultura, Ganadería y Desarrollo Rural. *Datos básicos del Sistema Nacional de Información Agropecuaria*, Centro de Estadística Agropecuaria; http://www.sagar.gob.mx/cea.htm (accessed 1998).
24. Instituto Nacional de Estadística, Geografía e Informática. *Sistema Municipal de Base de Datos*; http://www.inegi.gob.mx/homepara/estadistica/simbad/simbad.html (accessed 1998).
25. Mendoza, A.; Mejia, G.M.; Russell, A.G. In *Proceedings of the 91st Annual Meeting of the Air & Waste Management Association*; A&WMA: Pittsburgh, PA, 1998; paper no. 98-MP30.05.
26. Iqbal, M. *An Introduction to Solar Radiation*; Academic Press: New York, 1983; pp 202-210.
27. Goodin, W.R.; McRae, G.J.; Seinfeld, J.H. *J. Appl. Meteorol.* **1979**, *18*, 761-771.
28. Harley, R.A.; Russell, A.G.; McRae, G.J.; Cass, G.R.; Seinfeld, J.H. *Environ. Sci. Technol.* **1993**, *27*, 378-388.
29. Yang, Y.-J.; Mendoza, A.; Russell, A.G. In *Proceedings of the 91st Annual Meeting of the Air & Waste Management Association*; A&WMA: Pittsburgh, PA, 1998; paper no. 98-RP90B.03.
30. Grossi, P.; Giovannoni, J.-M.; Russell, A.G. *J. Appl. Meteorol.* **1996**, *35*, 993-1008.
31. Kuebler, J.; Giovannoni, J.-M.; Russell, A.G. *Atmos. Environ.*. **1996**, *30*, 951-966.
32. McRae, G.; Goodin, W.; Seinfeld, J.H. *Atmos. Environ.* **1982**, *16*, 679-696.
33. Russell, A.G.; McCue, K.F.; Cass, G.R. *Environ. Sci. Technol.* **1988**, *22*, 263-518.
34. Russell, A.G.; McRae, G.J.; Cass, G.R. *Atmos. Environ.* **1983**, *17*, 949-964.
35. Carter, W.P.L. *Atmos. Environ.* **1990**, *24A*, 481-518.
36. Yang, Y.-J.; Wilkinson, J.G.; Russell, A.G. *Environ. Sci. Technol.* **1997**, *31*, 2859-2868.
37. Yang, Y.-J.; Odman, M.T.; Russell, A.G. In *Proceedings of the 91st Annual Meeting of the Air & Waste Management Association*; A&WMA: Pittsburgh, PA, 1998; paper no. 98-WP76A.06.
38. Tesche, T.W.; Georgopoulos, P.; Seinfeld, J.H.; Cass, G.; Lurmann, F.L.; Roth, P.M. *Improvement of Procedures for Evaluating Photochemical Models;* Report prepared by Radian Corporation for the State of California Air Resources Board, Sacramento, CA, 1990.
39. Mejia, G.M.; Cortes, E.I. In *Proceedings of the Second Inter-American Environmental Congress*; Monterrey, Mexico, 1995, pp 188-191.
40. Willmott, C.J. *Physical Geography* **1981**, *2*, 184-194.
41. Willmott, C.J.; Ackleson, S.G.; Davis, R.E.; Feddema, J.J.; Klink, K. M.; Legates, D.R.; O'Donnell, J.; Rowe, C.M. *J. Geophys. Res.* **1985**, *90(C5)*, 8995-9005.
42. Trainer, M.; Williams, E.J.; Parrish, D.D.; Buhr, M.P.; Allwine, E.J.; Westberg, F.C.; Liu, S.C. *Nature* **1987**, *329*, 705-707.
43. Seinfeld, J.H.; Pandis, S.N. *Atmospheric Chemistry and Physics: From Air Pollution to Climate Change*; John Wiley & Sons: New York, 1998.
44. Sillman, S.; Logan, J.; Wofsy, S. *J. Geophys. Res.* **1990**, *95*, 1837-1851.
45. Roselle, S.J.; Pierce, T.E.; Schere, K.L. *J. Geophys. Res.* **1991**, *96*, 7371-7394.
46. Simpson, D. *J. Geophys. Res.* **1995**, *100*, 22891-22906.

About the Authors

Alberto Mendoza-Dominguez (corresponding author) and James G. Wilkinson are Ph.D. candidates, Yueh-Jiun Yang a post-doctoral fellow, and Armistead G. Russell the Georgia Power Distinguished Professor, all at the School of Civil and Environmental Engineering, Georgia Institute of Technology, Atlanta, GA 30332.